Transport of tracers and pesticides through fractured clayey till: Large Undisturbed Column (LUC) experiments and model-based interpretation

Mosthaf, Klaus; Rolle, Massimo; Petursdottir, U.; Aamand, J.; Jørgensen, Peter Rene

Published in:
Water Resources Research

Link to article, DOI:
10.1029/2020WR028019

Publication date:
2021

Document Version
Peer reviewed version

Transport of tracers and pesticides through fractured clayey till: Large Undisturbed Column (LUC) experiments and model-based interpretation

K. Mosthaf[1,2], M. Rolle[1], U. Petursdottir[1], J. Aamand[2] and P. R. Jørgensen[3]

[1]DTU Environment, Technical University of Denmark, Bygningstorvet, 2800 Kgs. Lyngby, Denmark.

[2]Geological Survey of Denmark and Greenland, Øster Voldgade 10, 1350 Copenhagen, Denmark.

[3]GEOZ ApS, Klintebakken 9, DK-3520 Farum, Denmark.

Corresponding author: Klaus Mosthaf (klmos@env.dtu.dk)

Key Points:

- Tracer and pesticide transport experiments in water-saturated LUCs with visually similar clayey tills showed contrasting behavior
- Interpretation of LUC setups with 3D DFM model including nonequilibrium sorption kinetics based on detailed experimental characterization
- DFM modeling of field conditions using LUC parameters to investigate vertical pesticide migration through surficial clayey till aquitards

Keywords: 1829 Groundwater hydrology, 1832 Groundwater transport, 1847 Modeling (1952, 4316), 5104 Fracture and flow, 5139 Transport properties

This article has been accepted for publication and undergone full peer review but has not been through the copyediting, typesetting, pagination and proofreading process, which may lead to differences between this version and the Version of Record. Please cite this article as doi: 10.1029/2020WR028019.

Abstract

Leaching of contaminants through fractured aquitards such as clayey tills may occur due to typically slow matrix advection and diffusion, or it can be dramatically enhanced in the presence of preferential flow through fractures and macropores. Sorption also plays a crucial role since it can significantly impact contaminant leaching and residence times. These different mass-transfer mechanisms imply a distinct transport behavior and very different time scales for contaminant leaching towards underlying aquifer systems. However, the prevalent controls on contaminant transport and their effects are difficult to assess. This paper shows a detailed characterization of flow and transport processes under water-saturated conditions in two large undisturbed columns (LUCs) collected from two visually similar fractured/macroporous clayey tills typical for the northern hemisphere. Flow-through tracer and pesticide experiments revealed a contrasting transport behavior. In one column, transport through fractures/macropores was dominant, whereas matrix advection and diffusion had a distinct influence on solute transport in the other column. Detailed 3D discrete-fracture-matrix models were developed to illuminate prevalent controls on contaminant transport and to quantitatively interpret the flow-through experiments with a minimal number of fitting parameters. Nonequilibrium sorption kinetics were included to reproduce the transport behavior of the considered pesticide. The parameters determined from the two LUC experiments were integrated in a vertical cross-section model to investigate the influence of varying fracture properties on vertical solute transport through surficial clayey till aquitards. The analysis showed that small fracture apertures in deeper parts of the aquitard could substantially prolong solute migration times and control solute fluxes.

1 Introduction

Glacial deposits such as clayey tills are often found in the upper geological layers in many countries of the northern hemisphere (Høyer et al., 2019; Jørgensen et al., 2002; Kim et al., 2017; McKay, Gillham, et al., 1993; Parker et al., 1994; Young et al., 2021). Usually, clayey tills have a low hydraulic conductivity and can slow down solute migration or even act as a barrier for contaminant leaching towards groundwater bodies (Chapman et al., 2018). However, pesticides have frequently been found in aquifers underlying supposedly protective geological layers, such as clayey tills (Bradbury et al., 2006; Cherry et al., 2006; Helmke et al., 2005b; Jørgensen et al., 2016; Jørgensen & Fredericia, 1992; Malaguerra et al., 2012). Once they reach the aquifer, pesticides and their degradation products can threaten groundwater quality and may even necessitate shutting down water supply wells. For instance, pesticides and their metabolites were found in about 41% of 2556 monitored drinking water wells in 2018 in Denmark, with more than 11 % exceeding the EU limit values of 0.1 µg/l for pesticides in drinking water (Council of the European Union, 1998; Thorling et al., 2019), causing the shutdown of many water supply wells.

Flow patterns in glacial clayey tills are often very heterogeneous and complex (Jørgensen et al., 2002; Rosenbom et al., 2008). In addition to matrix heterogeneities like sand layers and sand lenses (Kessler et al., 2012), fractures and macropores can act as preferential transport pathways for contaminants and considerably shorten travel times and increase solute fluxes (Batany et al., 2019; Fjordbøge et al., 2017; Harrison et al., 1992; Looms et al., 2018). Due to the low hydraulic conductivity of the clayey-till matrix, there is often a strong contrast between fracture and matrix conductivity. Hence, advective transport in open macropores and major fractures happens relatively fast compared to transport in the clayey till matrix where diffusion is the dominant transport process (Jin et al., 2014; Koestel & Larsbo, 2014; Muniruzzaman & Rolle, 2019; Parker et al., 2008; Rolle et al., 2013) However, the appearance of large-aperture fractures (few tens to a few hundred µm) and

macropores (e.g., earthworm burrows, root channels) is often limited to the uppermost few meters of the soils. Below that the fracture density often decreases (Harrar et al., 2007; Jørgensen, McKay, et al., 2004; Mckay & Fredericia, 1995) and smaller apertures can be observed (Helmke et al., 2005a; Young et al., 2019), with few to no macropores present. For long residence times, matrix diffusion can considerably slow down contaminant transport through fractures due to a continuous transfer of the solute from the fractures to the matrix (e.g., Carrera et al., 1998; Grisak & Pickens, 1980; Lipson et al., 2005; Mosthaf et al., 2018), with the solute flux into the matrix that may be enhanced by sorption to solid phase organic carbon (e.g., Parker et al., 1994). Once diffused into the matrix, the contaminant can be stored and released over a long time period due to the reversal of concentration gradients causing back-diffusion from the matrix to the preferential flow paths (Chapman & Parker, 2005; Sale et al., 2013). Furthermore, when the hydraulic conductivity contrast between fractures and matrix is small, matrix advection may also have an important influence on contaminant migration. The interplay between matrix advection/diffusion and advection in fractures/macropores can be decisive in the risk assessment of contaminant leaching to groundwater bodies. In addition to advective and diffusive processes, sorption to the fracture wall and the matrix is important since it can strongly delay the migration in the fractures and through the matrix and enhance the mass transfer between fractures and matrix. Moreover, it can reduce concentrations and mass fluxes of dissolved contaminants to an underlying aquifer.

The determination of properties controlling vertical flow and transport in fractured clayey tills is a challenging task, because flow in clayey till often shows a heterogeneous flow pattern caused by natural small-scale heterogeneities and interconnected preferential flow paths. For laboratory experiments, a challenge is to preserve the geological heterogeneity and the integrity of fractures and macropores. Field experiments such as pumping tests, infiltration experiments or geophysical methods (Bradbury et al., 2006) usually yield average parameters, which make it difficult to investigate the role of the individual transport paths in the geological formation (e.g., fractures, macropores, textural heterogeneities). The large undisturbed column (LUC) method is a useful setup for a detailed analysis of flow and transport processes in large samples excavated from clayey tills (Jørgensen et al., 2019). The LUC method aims at a minimal disturbance of natural fractures and at mimicking field conditions (confining stress and temperature) in the laboratory. The method allows for the determination of parameters required for assessing the risk for leaching of contaminants, such as pesticides, chlorinated organic compounds or nitrate (Jørgensen, Broholm, et al., 1998; Jørgensen, McKay, et al., 2004; Jørgensen, Urup, et al., 2004; O'Hara et al., 2000). Typical features such as macropores, fractures and clayey-till matrix properties and their influence on solute transport can be investigated, since such features are well represented and well defined in the large column samples (diameter of 0.5 m and height of 0.5 m).

The objective of this study is to investigate transport of a conservative tracer and a sorbing pesticide through macroporous/fractured clayey till settings revealing contrasting transport conditions, which are both typical for this environment. Therefore, we performed LUC experiments with two visually similar clayey tills from two field sites and different depths below ground surface. We excavated one column from approximately 2 m below ground surface (bgs), the other one from approximately 5.5 m bgs. The detailed characterization highlighted different fracture properties, distinct interaction between flow and transport processes in fractures and matrix, and different sorption/desorption behavior of the solutes in the two columns. We developed a 3D discrete-fracture-matrix (DFM) model to quantitatively interpret the flow-through experiments and to illuminate key processes controlling tracer and pesticide transport. Finally, we applied the LUC experimentally-

derived parameters using process-based DFM modeling in a 2D cross-section. The 2D DFM model allowed us to investigate possible vertical transport scenarios representative of field conditions with focus on potential bottlenecks controlling vertical transport in clayey-till aquitards and, thus, the risk of contamination to underlying aquifer systems.

2 Materials and Methods

2.1 Field sites and column samples

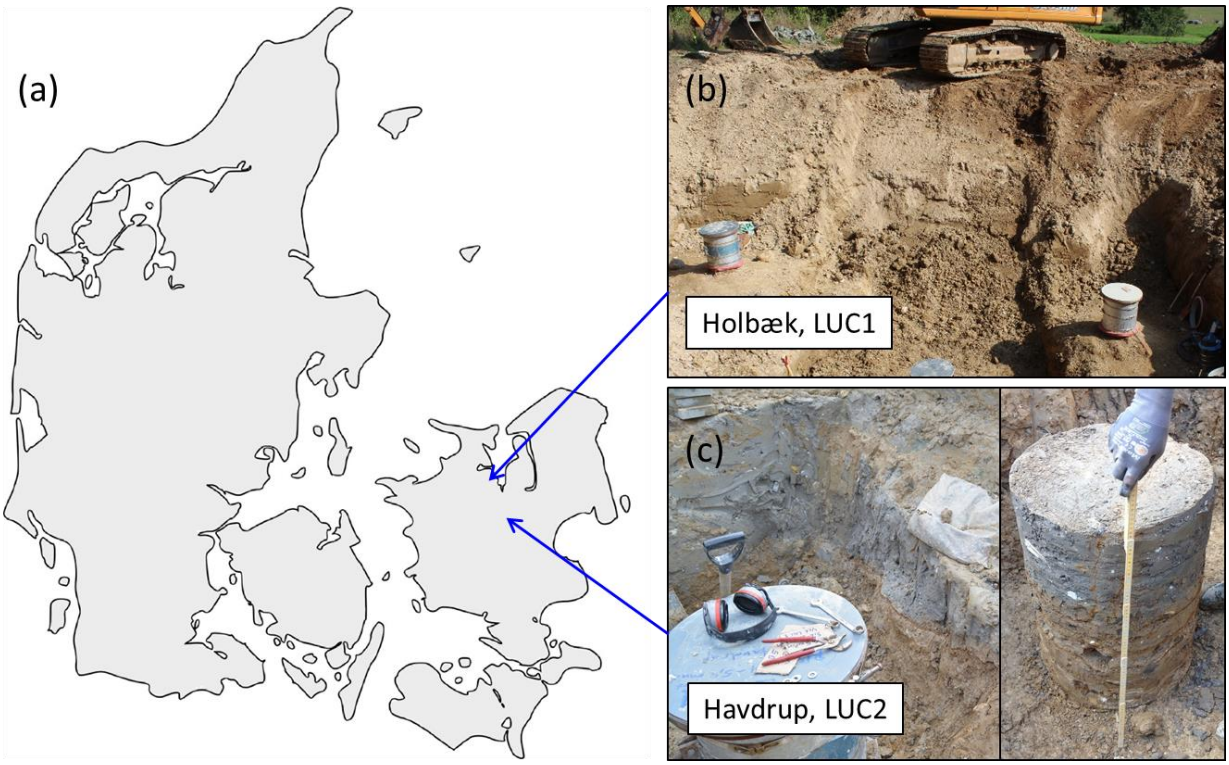

Figure 1. (a) Map of Denmark with the location of the considered field sites. **(b)** Photograph of the excavation site at Holbæk with LUC1 (1.95-2.38 m bgs) on the left. **(c)** Photographs of the excavation at Havdrup (LUC2, 5.4-5.9 m bgs) with grey reduced clayey till overlying brownish clay till.

Two field sites in Zealand, eastern Denmark, with Quaternary clayey till were considered: Havdrup and Holbæk (**Figure 1**). They are located approximately 35 km apart and have near-surface layers of glacial clayey till with fractures and macropores. The field sites have characteristics of clayey-till aquitards that can be typically found in Zealand, Denmark and, more generally, in the northern hemisphere. Large undisturbed columns (LUC) with a diameter of 0.5 m and height of 0.5 m were excavated at each field site for testing in the laboratory. The column LUC1 from Holbæk was excavated from a shallow depth (1.95-2.45 m bgs), while LUC2 from Havdrup was extracted from 5.4 to 5.9 m bgs. The LUC method was developed and applied in several studies (Jørgensen, McKay, et al., 1998; Jørgensen, Urup, et al., 2004; O'Hara et al., 2000). A detailed and comprehensive description of the LUC approach is provided by Jørgensen et al. (2019).

Top views on clayey-till slices from both LUCs are shown in **Figure 2**, illustrating the main features of each large undisturbed column. LUC1 (1.95 to 2.38 m bgs) from Holbæk had a relatively uniform yellowish-brown clayey-till matrix with a complex connected fracture network dominated by two main, conductive fractures that were continuous throughout the column (**Figure 2a**). The major fractures contained root channels that

followed the fracture paths. Moreover, some solitary macropores were observed. LUC2 (5.4 to 5.9 m bgs) from the Havdrup site contained one major vertical fracture through the column (**Figure 2b**) with embedded macropores partially filled with Fe/Mn-oxide, and a few minor fractures. The oxidized brownish clayey-till matrix in the lower half of LUC2 (**Figure 1c**) was more heterogeneous than in LUC1 with two visible clayey till types: A brownish sandy clayey till was found next to a less permeable brownish grey clayey till, overlain by low-conductivity reduced grey clayey till (see also **Figure 1c**). Thin horizontal sand layers provided a connection between the main fracture and the more conductive sandy clayey till.

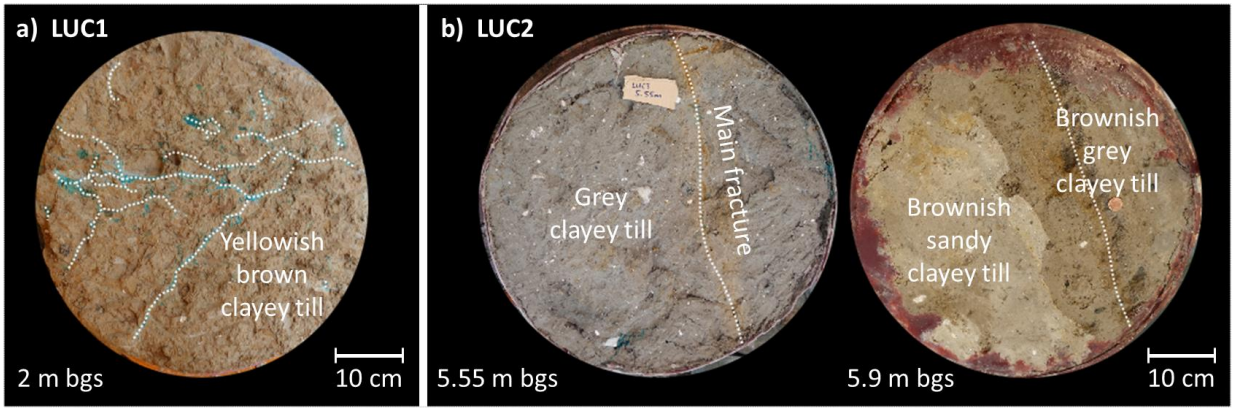

Figure 2. (a) Top view of a clayey-till slice from LUC1 with several fractures stained by the dye tracer brilliant blue and indicated by the white dotted lines. **(b)** Top view on two slices from LUC2 with one main vertical fracture and different clay types. The red-brown areas at the rim of the column, particularly visible at 5.9 m bgs is solidified polyurethane used to prevent or minimize rim flow.

2.2 Laboratory experiments

The two LUCs from clayey tills were excavated and installed in the laboratory for further testing following the procedure described by Jørgensen et al. (2019). The experiments conducted with the two LUCs included the following steps:

- Hydraulic tests at fixed flow rates to determine the bulk hydraulic conductivity based on the observed hydraulic gradient (piezometers at inlet and outlet of the LUC);
- Long-term flow-through experiments with pulse injections of solutions containing a conservative ionic tracer (bromide) and a sorbing pesticide (tebuconazole), followed by a flushing period with tap water (similar chemical composition as the groundwater at the site);
- Injection of a dye tracer solution until visible breakthrough in the effluent water to determine active flow paths. These experiments were followed by dismantling and segmentation of the LUC, visual inspection of the column interior, and mapping of major hydrogeological features (fractures, macropores, clayey till types);
- Determination of matrix hydraulic conductivity, bulk density and porosity on subsamples from intact matrix portions of the LUC. These properties were determined with triaxial cell permeability tests (see **Table 1**).

We conducted long-term flow-through transport experiments to investigate the solute transport behavior in the two large clayey-till columns. The three solutes that we employed in the LUC experiments were bromide (from KBr), the fungicide tebuconazole (CAS number 107534-96-3) and the dye tracer Brilliant Blue FCF (Erioglaucin disodium salt, CAS number

3844-45-9). Bromide was chosen as the conservative solute whereas tebuconazole was selected as the sorbing solute. Tebuconazole is a fungicide that is widely used in Europe, Australia, USA and other countries in large field crops. The two compounds also have distinct compound-specific diffusion properties, which exert an important control on mass transfer in porous media (Rolle et al., 2018; Rolle & Kitanidis, 2014): bromide has a high aqueous diffusion coefficient ($D_{aq} = 2 \cdot 10^{-9}$ m^2/s) whereas tebuconazole has a considerably lower aqueous diffusivity ($D_{aq} = 3.7 \cdot 10^{-10}$ m^2/s, based on Worch (1993)). Tebuconazole does not undergo significant degradation but shows a strong sorption to organic material and clayey till. A brilliant blue solution with a concentration of 2 mg/L was used for the visualization of major flow paths after completing the flow-through tests with bromide and tebuconazole. Brilliant blue sorbs to the clayey-till matrix and dyes the flow paths blue (Flury & Flühler, 1995).

Table 1. Bulk and matrix hydraulic conductivities, dry bulk densities and porosities determined on subcores with constant head flow tests in a triaxial cell.

Clay & depth bgs	Hydraulic conductivity* (m/s)	Matrix porosity (-)	Dry bulk density (kg/m^3)
LUC1 – bulk	$4.1 \cdot 10^{-6}$		
Yellowish brown clay – 2 m	$1.5 \cdot 10^{-9}$	0.30	1870
Gravel infill	$5 \cdot 10^{-3}$	0.42	
LUC2 – bulk	$9.4 \cdot 10^{-9}$		
Grey clay – 5.5 m	$1.7 \cdot 10^{-9}$	0.23	2070
Brownish sandy clay – 5.8 m	$2.3 \cdot 10^{-8}$	0.31	1850
Brownish grey clay – 5.8 m	$4.9 \cdot 10^{-9}$	0.21	2130

*Average value for three measurements for each sample.

The long-term flow-through experiments on both LUCs had an injection period followed by flushing with clean tap water. Hence, matrix diffusion and sorption, as well as back diffusion and desorption took place and influenced the solute breakthrough curves. In LUC1, a solution with dissolved KBr (80 mg/L bromide) and tebuconazole (16.6 µg/L) was injected for 221.6 hours with a high average flowrate of 81 mm/day (663 ml/h) for the first 29.6 hours, mimicking strong infiltration caused by a heavy rainfall event. Then the average flowrate was lowered to 9.8 mm/day (80 ml/h) for the rest of the experiment. After 221.6 hours, the column was flushed with tap water with a continuous flowrate of 9.8 mm/day (80 ml/h). The observed average hydraulic head gradient was approximately 0.23 m/m for the high flowrate, which is in the range of observed vertical gradients in clayey till aquifers (Harrar et al., 2007). Following the flushing period, the dye tracer brilliant blue was injected for 8 hours with an average flow rate of 47 mm/day.

In the LUC2 experiment, a constant flowrate of 2.44 mm/day (20 ml/h) was applied. The hydraulic gradient was approximately 3 m/m. First, a tebuconazole solution (20 µg/L) was injected for 359.2 hours (14.97 days), followed by 342.5 hours (14.27 days) of flushing with clean water at the same flow rate. Afterwards, the same procedure was repeated with a bromide solution (105 mg/L). Finally, brilliant blue was injected over a period of 181 hours at the flow rate of 20 ml/h.

The bromide concentrations in the effluent water were measured with ion chromatography (IC Metrohm, Detector 819) and a bromide-selective electrode (Br 800,

WTW). The tebuconazole concentrations were determined with LC-MS/MS analysis in a certified external laboratory. Brilliant blue was visually inspected after completing the flow-through experiments, opening and segmenting the columns. The average trace length of the active preferential flow paths was determined based on fractures observed during the segmentation of the column and, if applicable, by brilliant blue dyed traces along the fractures.

3 Flow and transport modeling

The flow and transport experiments on the LUC columns were evaluated with multidimensional discrete-fracture modeling performed with the finite-element code COMSOL Multiphysics®. Discrete-fracture-matrix (DFM) simulations were setup to solve flow and transport in fractures and the low-conductivity clayey-till matrices. In the models, fractures were resolved as discrete and lower-dimensional objects with planar geometry and mean hydraulic fracture aperture d_f, embedded in a matrix continuum. Blessent et al. (2014) found that DFM models give a good and robust representation of transport in fractured clayey tills and are applicable over a large parameter range without need for recalibration for different flow conditions. The fracture geometries in the present study were based on the observed fracture patterns with idealized and linearized fracture setups (i.e., the observed fracture trace length in the experiment) instead of an undulating fracture pattern in order to limit the meshing and the computational cost. Simulations with more tortuous fracture patterns and the same fracture trace length showed only small impacts on the simulated breakthrough curves, as also observed by Allaire et al. (2002).

A coupled set of equations was solved for each continuum (fractures and matrix). In the matrix continuum, a flow equation based on Darcy's law and a transport equation (advection-dispersion equation) were solved. A sequence of steady-state flow fields was employed to describe flow, since the transition time between the flow changes was short compared to the duration of the experiment. The steady-state groundwater flow equation in the matrix was formulated as:

$$\nabla \cdot (-\mathbf{K}\nabla h) = 0 \tag{1}$$

where **K** is the hydraulic conductivity tensor (assumed isotropic in the matrix) and h is the hydraulic head.

We used the cubic law (Snow, 1969; Witherspoon et al., 1980) to describe fracture flow. This law gives a cubic relation between hydraulic fracture aperture d_f (often denoted as $2b$, twice the half-aperture b) and water discharge (Chambon et al., 2010). Such relation can be inserted in the steady-state continuity equation, yielding:

$$\nabla \cdot d_\mathrm{f}\boldsymbol{v}_\mathrm{f} = \nabla \cdot (-d_\mathrm{f}K_\mathrm{f}\nabla_\mathrm{T}h) = \nabla \cdot \left(-{d_\mathrm{f}}^3 \frac{\rho_\mathrm{w} g}{12\mu_\mathrm{w}} \nabla_\mathrm{T}h\right) = 0 \tag{2}$$

where $\boldsymbol{v}_\mathrm{f}$ is the flow velocity in an open fracture (fracture porosity of 1), ∇_T is the gradient in the tangential directions and $K_\mathrm{f} = {d_\mathrm{f}}^2 \rho_\mathrm{w} g/(12\mu_\mathrm{w})$ is the fracture hydraulic conductivity, where ρ_w and μ_w are the density and viscosity of water.

Solute transport in the matrix is described by the advection-dispersion-sorption equation:

$$\phi \frac{\partial c}{\partial t} + \rho_\mathrm{b} \frac{\partial c_\mathrm{s}}{\partial t} + \nabla \cdot (\phi c \boldsymbol{v}) - \nabla \cdot (\phi \mathbf{D}_\mathrm{eff} \nabla c) = 0 \tag{3}$$

with the porosity ϕ, the solute concentration c, the bulk density ρ_b, the fluid velocity $\boldsymbol{v}$, the effective hydrodynamic dispersion tensor $\mathbf{D}_\mathrm{eff}$, the sorbed concentration $c_s = cK_\mathrm{d}$ assuming

linear equilibrium sorption, where K_d is the distribution coefficient. For the pesticide compound used in this study, a kinetic sorption model (Brusseau et al., 1989; Zheng & Bennett, 2002) was required. An additional equation describes the kinetic exchange of mass between the fluid (dissolved compound) and the bulk material (sorbed compound):

$$\rho_b \frac{\partial c_s}{\partial t} = \beta(c - c_s/K_d) \tag{4}$$

We defined different sorption kinetic parameters β_1 and β_2 for sorption and desorption from and to the matrix:

Sorption: $(c - c_s/K_d) \geq 0: \beta = \beta_1$

Desorption: $(c - c_s/K_d) < 0: \beta = \beta_2$

An advection-dispersion equation also describes solute transport in the fracture. We defined the transport equation for a solute through an open fracture as:

$$d_f R_f \frac{\partial c}{\partial t} + \nabla \cdot (d_f \boldsymbol{v}_f c) - \nabla \cdot (d_f D_f \nabla_T c) = 0 \tag{5}$$

where R_f is the retardation factor to account for equilibrium sorption on the fracture walls and D_f is the longitudinal hydrodynamic dispersion coefficient along the fracture, which can be approximated as $D_f = D_{aq} + (\boldsymbol{v}_f d_f)^2 (210 D_{aq})^{-1}$(Wang et al., 2012). The continuity of water and solute fluxes and the continuity of the primary variables, the hydraulic heads and solute concentrations, at the fracture-matrix interface provide the coupling between fractures and matrix.

The mathematical model is based on the following assumptions: (i) water flow can be described by a set of steady-state flow fields, (ii) the system is fully water-saturated, (iii) no degradation is happening, (iv) fracture flow and transport are approximated with the cubic law for the mean hydraulic fracture conductivity, (v) the fracture representation can be linearized and idealized based on the experimentally determined fracture trace length.

3.1 Model setup for the LUC experiments

The 3D model geometry of a LUC consists of a cylinder with a diameter and height of 0.5 m, with four inlet ports at the bottom (specified flux boundary conditions for flow and transport), and four outlet ports at the top of the system (fixed hydraulic head and outflow boundary condition for transport). Note that the clayey-till column was installed upside-down in the physical experiment (**Figure 3a**) and that the flow in the LUC setup was upward directed, therefore it represents downwards infiltration of water in the field. This is to facilitate the removal of entrapped air in the column. The numerical model was setup accordingly with flow from the bottom to the top (**Figure 3b**). The observed conductive fractures were represented as planes parallel to each other and assumed equal in aperture, with a constant hydraulic aperture derived by calibrating the hydraulic flow model to the flow rate and head gradient through the clayey till (**Table 2**).

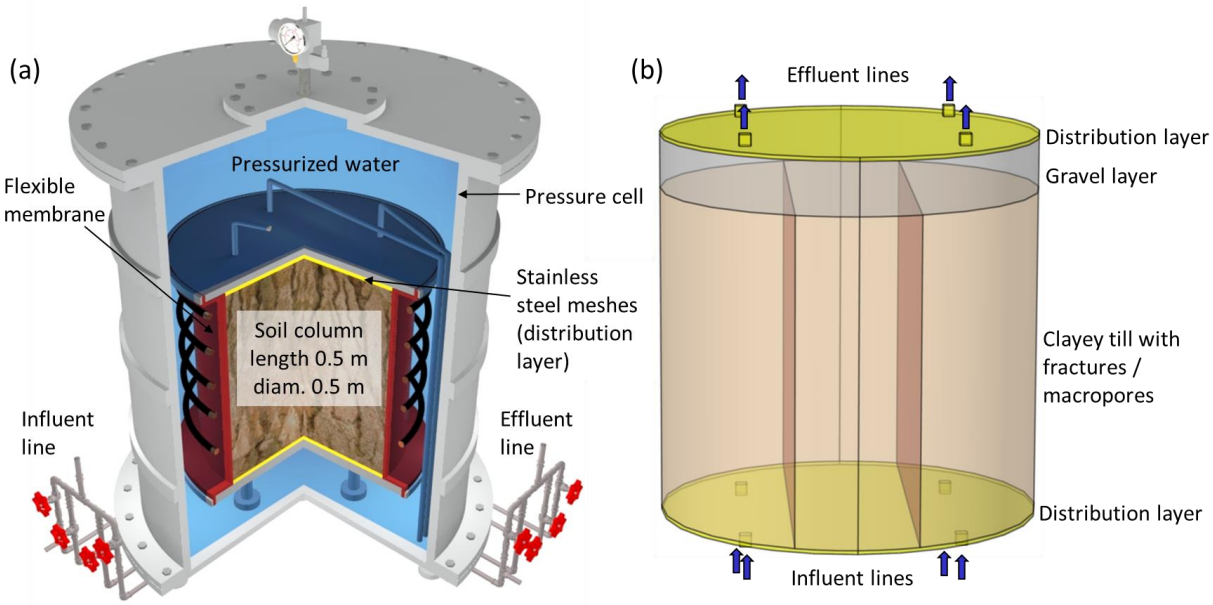

Figure 3. (a) Setup of a Large Undisturbed Column (LUC) experiment in the lab, modified after Jørgensen et al. (Jørgensen et al., 2019), reprinted from *Groundwater* with permission of the National Ground Water Association. Copyright 2019. **(b)** Model setup of the LUC system with four inlet and four outlet ports, distribution layers and the matrix sample with fracture planes. This example illustrates the setup for LUC1 including two vertical fractures and a gravel infill on top.

Table 2. Overview of parameters used in the two 3D DFM models for LUC1 and LUC2. Complementary parameters can be found in Table S1 in the Supporting Information.

Property	LUC1	LUC2	Unit	Source
Flow rate	81 / 9.8	2.44	mm/day	Experiment
Vertical hydraulic gradient	0.23	3	m/m	Experiment
Bulk hydraulic conductivity	$4.1 \cdot 10^{-6}$	$9.4 \cdot 10^{-9}$	m/s	Experiment
Fracture trace length	0.95	0.43	m	Experiment + fitted
Average hydraulic fracture aperture	110.6	18.5 / 10	µm	Experiment + fitted[a]
Effective stress	42.5	83.8	kPa	Experiment
Inlet concentration bromide	1	1	mg/L	Experiment
Inlet concentration tebuconazole	0.02	0.02	mg/L	Experiment
Aq. diffusion coefficient bromide	$2 \cdot 10^{-9}$	$2 \cdot 10^{-9}$	m^2/s	Cussler (2009)
Aq. diffusion coefficient tebuconazole	$3.7 \cdot 10^{-10}$	$3.7 \cdot 10^{-10}$	m^2/s	Worch (1993)
Dispersivities (α_L, α_T, α_V) in matrix	1, 1, 0.2	1, 1, 0.2	mm	Estimate
Distribution coeff. tebuconazole (K_d)	11	11	L/kg	Fitted[b]
Nonequilibrium sorption coeff. (β_1)	$5 \cdot 10^{-4}$	$5 \cdot 10^{-4}$	1/s	Fitted
Nonequilirbium desorption coeff. (β_2)	$1 \cdot 10^{-5}$	$1 \cdot 10^{-5}$	1/s	Fitted

[a] Average hydraulic aperture as determined with the 3D DFM model. In LUC2, the fracture aperture was determined as 18.5 µm in the lower 0.4 m and 10 µm above.
[b] Determined within the range of a similar clayey till in Albers et al. (2018).

On the top and the bottom of the clay column, distribution layers with a thickness of 5 mm were included in the 3D model to facilitate the distribution of flow across the ends of the LUC according to the hydraulic conductivity of fractures and matrix. Such permeable distribution layers (hydraulic conductivity: 0.1 m/s) mimic the effect of the steel meshes that were placed on each side of the clay column and the volume of the influent lines in the experimental setup.

The conceptualization and the model setup for each column are based on the segmentation and slicing of the columns, and are shown in **Figure 4** as cross sections through the center of the two columns. The complex fracture network observed in LUC1 was simplified to two parallel vertical fractures with a hydraulic trace length of 0.95 m according to the experiment. The model for LUC1 includes a 7 cm thick medium-fine gravel layer on top of the setup. This filling was added in the physical experiment since, despite careful preparation and handling of the column, the lowest 7 cm of the clayey-till column (top in the LUC setup) had detached during the excavation at the field site. High conductivity ($5 \cdot 10^{-3}$ m/s) and no sorption were assigned to the gravel infill in the model.

The experimental investigation of LUC2 highlighted three different clayey tills (**Figure 4b**). However, the differences in the hydraulic properties between the reduced grey clayey till and the yellow grey clayey till in LUC2 were small and, therefore, not considered in the numerical model. Hence, two clayey tills were distinguished: the more conductive yellow sandy clayey till and the grey clayey till, which contained the main vertical fracture with a trace length of 0.43 m and equivalent hydraulic aperture of 18.5 µm. Two horizontal sand layers were included, a thin one (modeled as 2D fracture planes with d_f=8 µm, corresponding to a hydraulic conductivity K=$3.85 \cdot 10^{-5}$ m/s and unity porosity) at 5.70 m bgs and a thicker one (d_f=18.5 µm, K=$2.06 \cdot 10^{-4}$ m/s and unity porosity) at 5.80 m bgs, see **Table SI1**. The sand layers connect the main fracture with the yellow sandy clayey till.

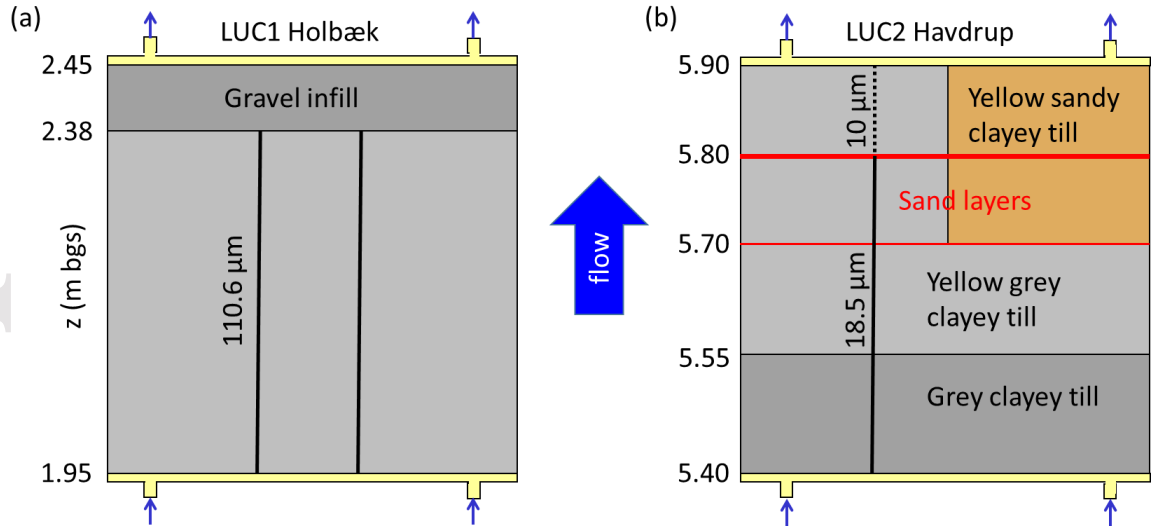

Figure 4. Schematic setup (central vertical cross section) of the model for **(a)** LUC1 and **(b)** LUC2.

Concentrations in the effluent water were computed as flux-averaged concentrations at the outlets, so they were comparable to the measured values. To minimize numerical dispersion and to avoid a mesh-dependent solution, the mesh was refined at locations, where steep gradients could be expected, i.e., at inlets and outlets, at the interface between materials with different hydraulic conductivity, and particularly around fractures. At the fractures, an octahedral boundary layer mesh was created with an initial element width perpendicular to

the fracture in the order of the fracture aperture (Weatherill et al., 2008). The initial element width was 200 µm for LUC1 and 50 µm for LUC2. From the fractures, the element size was exponentially enlarged from tens of micrometers to centimeters with a maximum element growth rate of 1.2 and with a transition from the octahedral to a tetrahedral mesh in the remaining domain. To reduce the computational costs, the vertical symmetry of the system was exploited and a half cylinder with in-/outlets and redistribution layers was simulated. This led to meshes with 4.3 million elements for LUC1 and 1.5 million elements for LUC2.

To calibrate the 3D flow and transport models, measured data including matrix hydraulic conductivities and porosities (from the matrix subsamples), and observed fracture traces extruded to vertical 3D surfaces were used as fixed simulation inputs, aiming for a minimal number of fitting parameters. Then, the 3D steady-state flow model was calibrated to the observed head difference between inflow and outflow by varying the average hydraulic aperture of the main fracture(s) with an automated optimization. Once the steady-state flow field was fixed, the 3D transport model was manually calibrated to the measured breakthrough curves of bromide using the steady-state flow field as an input. Finally, the K_d value of tebuconazole and nonequilibrium sorption coefficients were calibrated to the measured breakthrough curves. We considered different fracture trace lengths (within the observed ranges) and different conceptualizations in LUC2 (sand layers, heterogeneous matrix) and selected the ones reproducing the experiments best. The goodness of fit was quantified with the normalized root mean square error (NRMSE) between measured and simulated concentrations of the conservative and sorbing compounds in the effluent water (breakthrough curves).

3.2 Model setup of vertical cross sections representative of field conditions

Leaching of solutes through clayey-till profiles usually implies heterogeneous hydraulic properties, and often a decrease of fracture density and hydraulic apertures with depth is observed. This can shift the main transport from fractures to matrix and constrain the vertical solute fluxes. To investigate the effects of a reduction of the hydraulic aperture in a larger vertical cross section, we combined the two investigated LUCs extracted from different depths in a vertical 2D cross section, while keeping other parameters and the vertical hydraulic gradient constant. The two LUCs represent typical conditions at different depths and their combination represents a typical sequence in a clayey-till geology in the region of the considered field sites (Zealand, Denmark) and, more generally, in the northern hemisphere. We assigned the fracture properties of the two LUCs to portions in the cross section with the larger aperture values from LUC1 in the top part, i.e., fractures become narrower with increasing depth. This could be due to, e.g., a higher confining stress and less influence of biopores at greater depth (Nilsson et al., 2001; Sidle et al., 1998). The matrix properties in the two LUCs were similar and a uniform hydraulic matrix conductivity and porosity (K=2·10^{-9} m/s, ϕ=0.25) were applied to isolate the effect of the fracture narrowing.

Flow and transport simulations were run on 2D vertical cross sections with four equally spaced fractures on a domain width of 2 m, hence a spacing of 0.5 m according to the size of an LUC and as a spacing common in clayey tills (Jørgensen, McKay, et al., 2004). A periodic system was considered and symmetry was exploited by simulating one 0.5 m fracture-matrix interval and mirroring it horizontally for further evaluations of flow and transport in the considered domain. A depth interval of 4 m was simulated, covering the depth interval from LUC1 (ca. 2 m bgs) down to the depth of LUC2 (ca. 6 m bgs), representative for the solute leaching through a 4 m fractured clayey-till lithology to an underlying aquifer. A bromide and a tebuconazole solution with a concentration of 1 mg/L and 20 µg/L were continuously infiltrated from the top of the model domain with a hydraulic

gradient of 0.25 m/m (fixed hydraulic heads at the top and bottom boundaries with h_{top} = 5 m and h_{bottom} = 4 m for all cases). The vertical hydraulic gradient was chosen in the lower range of vertical gradients observed at piezometers (0-1 m/m) installed at different depths at the Havdrup field site, in which water levels were recorded for several months. The same diffusion and sorption parameters as for the LUC experiments (**Table 2**) were used in the transport simulations. To distribute the flow according to the hydraulic conductivity of the fractures and the matrix, a thin high-conductivity distribution layer was added at the top and the bottom of the domain. A mesh with 360k elements was employed with local refinement at the distribution layers and a boundary layer mesh with exponentially growing element size next to the fractures.

Five different setups were considered to analyze the effect of depth variations of the hydraulic fracture parameters on pesticide leaching informed by the LUCs and the observations at the field sites. The fracture parameters from the two LUC experiments, covering a typical range of the hydraulic fracture aperture, were assigned to portions of the vertical cross section: (i) a cross section with a large hydraulic fracture aperture (corresponding to LUC1) through the entire profile, (ii) a cross section with a small hydraulic aperture (corresponding to LUC2) through the entire profile, (iii) a fracture with an abrupt reduction of the aperture with depth after ¼, ½ and ¾ of the cross section, and (iv) a linear decrease of the aperture with depth. A schematic illustration of the different setups and cases for the simulated cross section is shown in Figure S1 (Supporting Information). Simulations were also run with tebuconazole with respective sorption and diffusion coefficients.

4 Results and discussion

4.1 Flow-through LUC experiments

The hydraulic tests of the two clayey-till columns from different depths revealed distinctly different hydraulic properties and flow characteristics (**Table 1** and **Table 2**), despite being from visually similar shallow clayey-till geologies. The bulk hydraulic conductivity of LUC1 from a shallower depth was 2-3 orders of magnitude higher than that of LUC2 ($4.1 \cdot 10^{-6}$ m/s vs. $9.4 \cdot 10^{-9}$ m/s), whereas the matrix properties in both columns were in a relatively smaller range with the matrix hydraulic conductivity varying by an order of magnitude ($1.5 \cdot 10^{-9}$ to $2.3 \cdot 10^{-8}$ m/s) and matrix porosity by less (21 to 31%, see **Table 1**). Values in these ranges were observed in previous work on glacial-derived clayey sediments including tills and diamicts (Fredericia, 1990; Jørgensen et al., 2016; Keller et al., 1988; McKay, Cherry, et al., 1993). The similar and much lower hydraulic conductivity values of the matrix in the two LUCs imply that the differences in the bulk hydraulic conductivity can be mainly attributed to different properties of the fractures, which control the extent of the preferential flow.

The average fracture trace length in combination with the determined matrix conductivity allowed for the determination of hydraulic fracture aperture values (**Table 2**) based on an optimization of the aperture in the 3D flow model. In LUC1, no staining of the membrane was observed upon segmentation of the column after the brilliant blue pulse injection, which allows excluding any rim flow. Brilliant blue staining was observed in both the fractures and the macropores (root channels) contained in the main fractures, showing significant channeling. Hence, a smaller portion of the geometrically measured trace length was used in the simulations (hydraulic trace length of 0.95 m compared to the average trace length of 1.35 m measured on the slices). The flow simulations allowed us to determine an average hydraulic aperture of 110.6 µm for the fractures in LUC1.

In LUC2, some brilliant blue staining of the membrane due to rim flow was visible in an interval length of ca. 10 cm in the lower part of the column (grey clayey till in Figure 4b). In the following it is assumed that the overall influence of rim flow was negligible also in this experiment and any contribution of such possible rim flow in the lower 10 cm of the column is lumped in the effective hydraulic fracture aperture. The main fracture in this column was embedded in the less conductive brownish and grey clayey tills and contained paleo root channels and some Fe/Mn-oxide precipitate filling. In the lower 15 cm of the LUC2 sample (5.40-5.55 m bgs), brilliant blue staining was observed in three 2-3 cm wide segments, related to macropores (root channels) along the main fracture, while brilliant blue was not observed in the fracture. The representation of such preferential flow features was carried out with a single fracture with the observed fracture trace length of 0.43 m and with a constant effective mean hydraulic aperture. Based on this approach, the average hydraulic aperture of the main fracture of the LUC2 (5.40-5.80 m bgs) was determined as 18.5 µm, entailing much slower and less flow through the fracture than in LUC1. For the upper 10 cm of the fracture (5.80-5.90 m bgs) no visible trace of brilliant blue was observed, indicating limited solute transport through this fracture interval, thus it was assumed that the average hydraulic aperture was smaller (10 µm). The brilliant blue injection and the subsequent segmentation revealed that thin horizontal sand layers at 5.70 m and 5.80 m bgs provided a hydraulic connection between the main fracture and the highly conductive brownish sandy clayey till which was identified as additional major transport pathway through the upper part of LUC2.

Based on a constant hydraulic gradient on the columns, the proportion of the total volumetric flux through the fractures was analyzed in the 3D modeling of the two LUC columns. This quantified the relative contribution of fractures and matrix to water flow and advective transport. The modeling results show that the water flow in LUC1 took place almost exclusively in fractures (99.96% of the total water flow), while in LUC2 about 83% of the total water flow happened through the main fracture, indicating a greater importance of the clayey-till matrix. In the upper part of the LUC (outflow side) with a smaller hydraulic aperture of 10 µm, the fractures only contributed with 18% to the total flux. This demonstrates that the greatest part of the water flow in the main fracture was redirected through the conductive horizontal sand layer to the more conductive brownish sandy clayey till.

The temporal evolution of the bromide and tebuconazole distribution within the LUCs is shown in **Figure 5**. In LUC1 (top row), bromide spreads quickly along the bottom distribution layer and migrates fast through the large-aperture fractures towards the top of the column, while only a small portion of the bromide diffuses into the matrix. The bromide passes the highly conductive gravel layer at the top and reaches the outlet ports within few hours (**Figure 5a**). When clean water is injected and the flushing phase of the experiment starts (**Figure 5b-c**), the bromide is rapidly flushed in the permeable flow paths, involving a rapid drop of the concentration in the fractures and some back-diffusion from the matrix. For tebuconazole (**Figure 5d-f**), a similar spreading behavior in the fractures can be observed. However, due to the strong sorption and less matrix diffusion (lower diffusivity of tebuconazole compared to bromide), the concentration values in the matrix are in general much lower than for bromide. Relative concentrations higher than 1% of the injected concentration can be mostly found next to the fractures and in the gravel layer.

The major transport pathway for bromide in LUC2 is also identified to be the main fracture (**Figure 5g**), until the solute reaches the horizontal sand layers (**Figure 5h-i**), where the bromide spreads also laterally and migrates through both the higher-conductivity brownish sandy clayey till and the smaller-aperture fracture filled with some precipitate. In LUC2, the interplay between advective transport in the fractures, matrix diffusion and

sorption is different compared to LUC1. The strong sorption of tebuconazole leads to a slower propagation of the pesticide (**Figure 5j-l**), despite a lower diffusion coefficient, which results in less matrix diffusion. As in LUC1, the highest tebuconazole concentrations can be found close to the fractures, and the dissolved tebuconazole concentrations in the matrix are much lower as for bromide. After 480 hours (**Figure 5l)**, the tebuconazole concentrations at the outlets is still below 1% of the injected concentration.

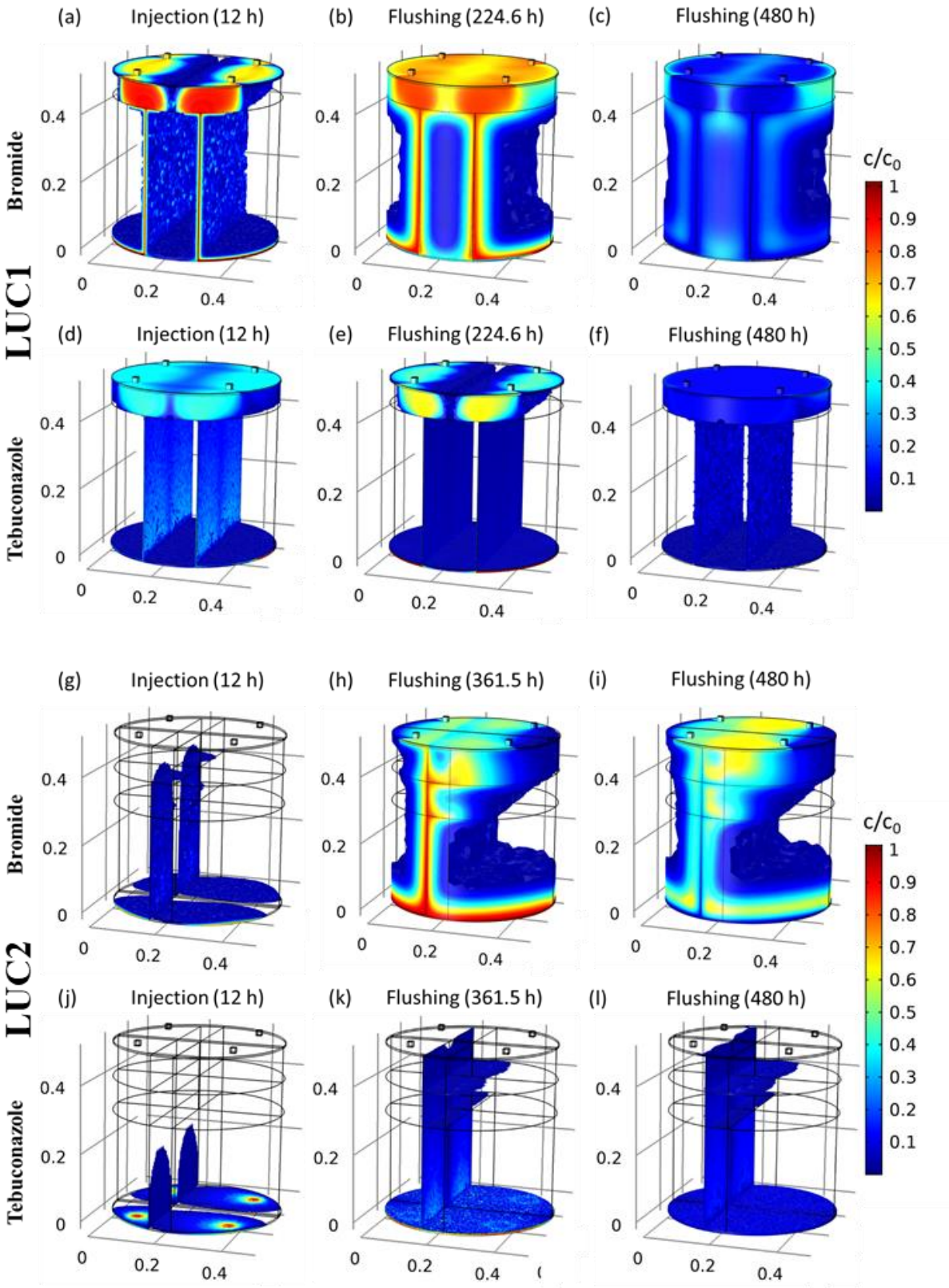

Figure 5. Simulated dissolved bromide and tebuconazole concentration distributions in LUC1 (a-f) and LUC2 (g-l) during the injection (a, d, g, j), at the beginning of the flushing period (b, e, h, k), and after a longer period of flushing (c, f, i, l). The flow is directed upwards. The color maps show relative concentrations higher than 1% of the injected values.

Figure 6 shows the measured and simulated breakthrough concentrations of bromide and tebuconazole in the effluent water of the two LUCs. In the simulated LUC1 experiment (**Figure 6a**) both solutes are very quickly transported through the fractures, and the concentrations at the outflow increase rapidly after the injection is started with 81 mm/day. The relative bromide concentration in the effluent water reached about 85% of the injected concentration before the flow rate was lowered to 9.8 mm/d. Then, the effluent concentration shows first a decrease, because there is a slight shift from fracture advection towards matrix diffusion at lower flow velocities. The lower flow rate and the increased residence time of the solutes lead to a stronger diffusion from the fractures into the matrix and hence to lower solute concentrations in the effluent water. The effluent concentrations became higher again when the matrix concentration next to the fractures increased, thus reducing the concentration gradient and the diffusive flux from the fracture into the matrix. Finally, the concentrations of both solutes decreased; this is reflected in a long tailing of the breakthrough curve after the pulse injections of bromide and pesticide were stopped and the system was flushed with clean water.

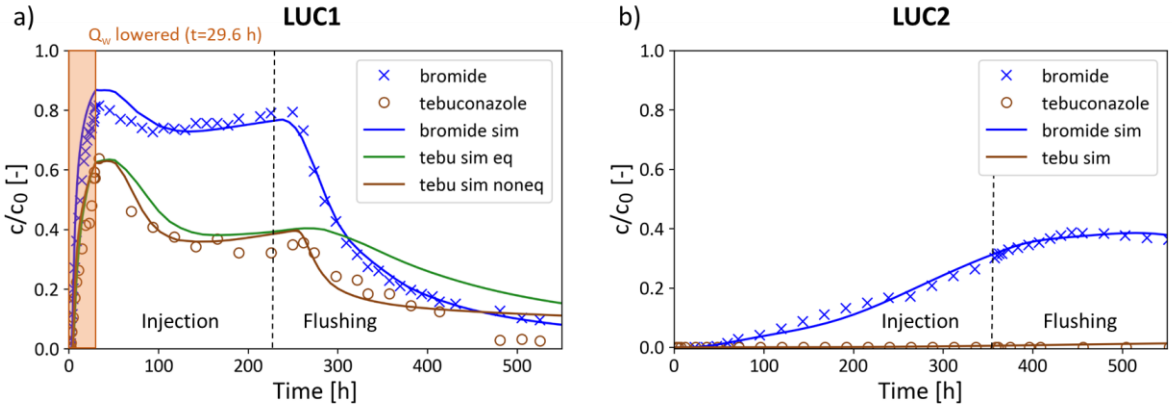

Figure 6. Simulated and measured breakthrough concentrations of bromide and tebuconazole in the effluent water for (a) LUC1 and (b) LUC2. The shaded area in (a) indicates the period with a high flow rate (81 mm/day), followed by a lower flow rate of 9.8 mm/day. The flow rate for the LUC2 experiment was constant (2.44 mm/day). The dashed vertical line indicates the time when the solute injection was stopped. Note that the flow rates and the hydraulic gradients were different in the two LUC experiments.

Despite a lower flow rate than in LUC1, a much higher head gradient established in LUC2. This is mainly attributable to less conductive fractures with smaller apertures. The bromide injected in LUC2 was detected at the outlet after about 10 hours (**Figure 6b**). Then, the breakthrough curve showed a slow and almost linear increase of the effluent concentration. When the tracer / pesticide injection was stopped after 359.2 hours, the concentrations at the outlet continued to slightly increase for another 40 hours until a peak concentration of approximately 40% of the injected concentration was reached and the effluent concentrations started to decrease. Tebuconazole concentrations stayed below the detection limit in the considered period of the LUC2 experiment due to a more important contribution of matrix diffusion resulting in increased fluxes from the fracture to the matrix and more effective pesticide retardation in this clayey till.

The fracture-advection dominated transport of bromide through LUC1 could be reproduced with the simplified model setup consisting of two parallel fractures with the average trace length based on the experimental characterization of the main fractures in the LUC monolith and an average hydraulic fracture aperture (NRMSE=0.067). The

breakthrough curve of tebuconazole showed lower concentrations compared to bromide due to sorption onto the matrix. The initial breakthrough behavior could be captured by a linear sorption model (NRMSE=0.091). However, when the injection was finished and the column was flushed with clean water, the equilibrium sorption model with K_d=11 L/kg overpredicted desorption and the resulting tailing of the curve did not match the data (green line in **Figure 6a**). The measured concentrations revealed only very little desorption and had a similar decreasing trend as bromide. This could be reproduced in the 3D model by using the nonequilibrium kinetic sorption model with K_d=11 L/kg, $\beta_1 = 5 \cdot 10^{-4}$ 1/s and $\beta_2 = 1 \cdot 10^{-5}$ 1/s (**Table 2**), which considerably improved the fit particularly in the tailing of the curve, after the tebuconazole injection was stopped (NRMSE=0.064). The distribution coefficient is within the range of 3-20 L/kg, as determined by Albers et al. (2018) at a similar clayey-till site. In LUC2, the water fluxes through fractures were of similar magnitude as the fluxes through the matrix. Thus, the hydraulic conductivity of the matrix, particularly in the more conductive sandy clayey till in the top of the column also played an important role on the observed solute transport. This is different from LUC1, where the accurate value of the matrix hydraulic conductivity had only a marginal influence on the solute breakthrough curves due to the strong conductivity contrast and the advection-dominated transport through the fractures. An idealized representation of the fractures with average hydraulic fracture apertures allowed in both cases the reproduction of the experimental observations.

4.2 Vertical cross-section simulations with fracture variation

The effect of vertical fracture variations on solute transport in a field scenario and the controls on vertical contaminant transport was investigated with simulations of extended vertical 2D cross sections with a combination of properties from both LUCs, with LUC1 representing clayey till conditions at shallow depths with macropores and large-aperture fractures, and LUC2 representing deeper parts with small-aperture fractures and small root channels. Six scenarios were considered, with different proportions of LUC1 and LUC2. The cases are named according to the length ratio of LUC1:LUC2, as summarized in Figure S1.

1) Continuous fractures with a constant aperture of 110.6 µm (purely LUC1, case 4:0) or 18.5 µm (purely LUC2, case 0:4),
2) Abrupt reduction of the aperture from 110.6 µm to 18.5 µm after 1 m, 2 m or 3 m from the top (cases 1:3, 2:2 and 3:1) as supported by fracture mapping in the excavations at the selected field sites,
3) Linear decrease of the fracture aperture from 110.6 µm to 18.5 µm (case lin).

First, the transport of bromide (no sorption, high diffusion coefficient) was simulated. **Figure 7a-c** show the evolution of the concentration in the cross sections. With a continuous hydraulic fracture aperture, the flow field shows a uniform pattern with depth. A large fracture aperture leads to a fast migration of the bromide in the fractures with a continuous transport into the matrix mainly driven by diffusion retarding its arrival but not preventing breakthrough (**Figure 7a**). With a smaller fracture aperture, the relative contribution of the diffusive transfer from the fractures into the matrix becomes stronger and the transport in the fractures happens at a considerably lower rate (**Figure 7c**)**.** When the hydraulic fracture aperture abruptly decreases, a part of the water is redirected out of the fracture into the matrix (**Figure 7b**, black arrows) similarly to the behavior of streamlines showing diverging patterns in flow defocusing zones in a heterogeneous porous medium (e.g., Muniruzzaman et al., 2014; Rolle et al., 2009). This effect was also observed along the entire fracture length for the case of a gradually narrowing fracture aperture (case "lin").

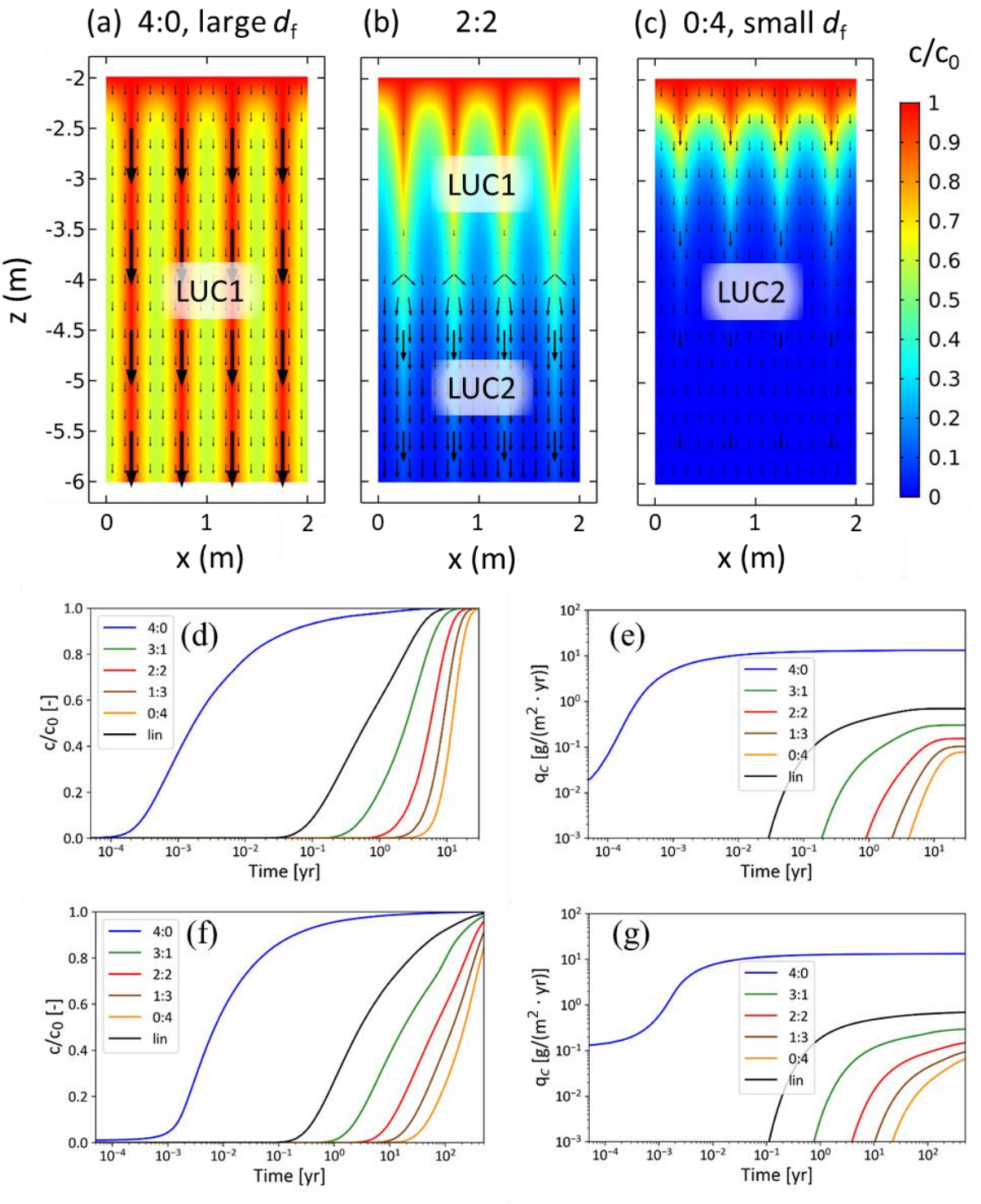

Figure 7. Analysis of the vertical transport scenarios with downwards-directed flow. The figures on the top show the concentration distribution of bromide for (a) a constant large aperture (110.6 µm, case 4:0), (b) an abrupt aperture decrease in the middle of the domain (4 m bgs, case 2:2) and (c) constant small aperture (18.5 µm, case 0:4), all after 2 years of continuous injection. The black arrows indicate velocity and flow directions in fractures and matrix; (d) shows the simulated effluent concentrations and (e) the respective effluent solute fluxes for bromide and (f) and (g) for tebuconazole, respectively.

Figure 7d shows the simulated bromide breakthrough concentrations at the bottom of the profile for different combinations of small and large hydraulic fracture apertures in the

vertical cross section. The simulated transport of tebuconazole followed the breakthrough pattern of bromide with a delay due to sorption to the matrix (**Figure 7f-g**).

The analysis of aperture variations with depth showed that portions of fractures with a small aperture delay the breakthrough considerably compared to a continuous fracture with a uniform large aperture. For the applied hydraulic gradient of 0.25 m/m, the time until the breakthrough of 1% of the inflow concentration at the bottom of the 4 m-deep cross section is approximately four years for a uniform aperture of 18.5 µm and about one hour for an aperture of 110.6 µm (4-5 orders of magnitude difference). When the upper 2 m had an aperture of 110.6 µm followed by 18.5 µm below (case 2:2), the time frame for solute breakthrough at the bottom of the profile was about one year and more similar to the case with a low aperture of 18.5 µm (case 0:4). The continuous decrease of the fracture aperture with depth (case "lin") lead to a relatively quick breakthrough, even faster than case 3:1. This is because of the nonlinear relation between fracture hydraulic conductivity and fracture hydraulic aperture (cubic law), the hydraulic fracture conductivities in case "lin" are larger than in case 3:1 in most of the domain. However, the breakthrough time in case "lin" is still two orders of magnitude longer and the breakthrough fluxes two orders of magnitude larger than for case 4:0 (aperture of 110.6 µm in the entire fracture). This analysis shows that small fracture apertures at greater depth can represent a bottleneck to vertical solute transport.

The effluent solute fluxes at the bottom of the cross section are plotted in **Figure 7e** and **Figure 7g** for a constant injection concentration of 1 mg/L bromide and tebuconazole. The contaminant fluxes for a continuous large fracture are more than two orders of magnitude higher than for a continuous small fracture. This is because, for the same hydraulic gradient, larger fracture apertures leads to a stronger advective contaminant transport with the water flux through the fractures. Additionally, the fast flow in large-aperture fractures leads to a lower relative contribution of the diffusive exchange with the matrix due to a shorter residence time of the solutes in the fractures. Again, the fluxes for the scenarios with a lower hydraulic fracture aperture at the bottom of the profile behave more similarly to the breakthrough in case of small-aperture fractures throughout the entire cross section. These results indicate that the parameters in deeper parts of the fractured clayey till control the vertical migration of solutes and are very relevant when assessing the risk of contaminant leaching through a clayey-till aquitard. Using uniform hydraulic properties in a vertical cross section and extrapolating hydraulic properties obtained from the top of the cross section of an aquitard to deeper parts can lead to a wrong approximation of breakthrough times and of water and solute fluxes.

5 Conclusions

In this study, we conducted two flow-through pesticide and tracer experiments in large undisturbed columns (LUC) from clayey till. We presented the results and interpreted the experiments with 3D discrete-fracture modeling. This yielded an improved hydrogeological understanding of the complex interplay between fractures and matrix with the processes of advection, diffusion and sorption on contaminant migration through clayey tills. Despite being from visually similar clayey-till lithologies, the two columns revealed distinctively different properties and flow and transport behavior. In the first column with an average hydraulic fracture aperture of approximately 110 µm, flow and transport mostly happened through the fractures and macropores (influenced by matrix diffusion when considering long time spans). The second column, excavated from a deeper clayey till (5 m bgs) and with average hydraulic fracture apertures of 10-18.5 µm, was characterized by more complex flow and transport through both fractures and clayey till matrix, particularly through a rather conductive sandy clayey till that was hydraulically connected to the main fracture by

thin horizontal sand layers. The time scales for vertical solute transport by a conservative, non-sorbing tracer differed by orders of magnitude (hours to days), which is due to the nonlinear relation between hydraulic fracture aperture and water flux in the fractures and to a different relative contribution of advective transport in the fractures and diffusive exchange of the solute with the matrix related to different residence times of the solute in the fractures. The results of the LUC experiments for the pesticide tebuconazole also showed the contrasting behavior between the two investigated clayey-till settings. Such behavior was the outcome of the interplay between advection, diffusion and sorption. The model-based description of the latter required a nonequilibrium formulation. The findings of this study are important for the assessment of the leaching behavior of solutes like pesticides through fractured clayey tills and highlight the importance of a good knowledge of fracture and matrix properties at several depths and hence a need of advanced experimental investigations.

Similarly to recent studies in physically heterogeneous porous media (Ye et al., 2015b, 2015a) the outcomes of this investigation show the importance of coupling multidimensional flow-through experiments with flow and transport modeling. This coupled approach could be extended to other low-conductivity fractured media and to other contaminants including solvents (Yu et al., 2018), charged inorganic compounds and emerging organic chemicals. Furthermore, the consideration of degradation reactions within the sorbed and aqueous phase would be a possible advancement of the presented approach for pesticides and other organic compounds undergoing biological and/or chemical transformations. The 3D discrete-fracture-matrix models with geometry and average parameters derived from accurate experimental characterization could successfully reproduce the breakthrough behavior of conservative and sorbing species under constant and variable flow conditions. In the reactive transport case, the model-based interpretation allowed us to estimate nonequilibrium sorption coefficients for the commonly used fungicide tebuconazole. In both LUC1 and LUC2 channeling occurred along larger aperture channels in the fractures. However, using an idealized fracture representation with average hydraulic aperture values lead to consistent results for both flow and transport in these cases. For the 3D simulation of larger-scale and complex field settings, massive parallel computing and advanced meshing techniques are required, as well as elaborate upscaling approaches. The LUC setup could be a useful tool to further test and develop such methods.

Transposing the experimental LUC findings to larger scale 2D model scenarios was instrumental to investigate the effect of vertical fracture variations on solute transport (pesticide leaching). This showed that a lower fracture aperture at depth strongly limits vertical transport and can considerably influence transport times and decrease contaminant fluxes. Moreover, a local narrowing of a fracture induces advective fluxes from the fractures into the matrix. The results of this experimental and model-based investigation are relevant for risk assessment and groundwater management since important aquifer systems can be present below clayey till aquitards, which are often thought and/or perceived to be impermeable and protective layers. Furthermore, this study with data from two apparently similar lithologies but quantitatively distinct properties shows that when assessing the risk of contaminant leaching through clayey-till lithologies, it is not enough to take measurements at one point and depth. The horizontal and vertical variability can be very strong and dramatically influence the leaching behavior. Single major fractures/macropores with large apertures may act as rapid transport pathways for the contaminants and dominate the contaminant transport over larger areas. This work highlights the benefit of extensive investigation based on multiple lines of evidence (Broholm et al., 2016; Parker et al., 2019) and on the combination of experimental observation with model-based interpretation, as well as the need of mapping connected hydrological features in clayey till geologies.

Acknowledgements

The measured and simulated effluent concentrations from the two LUC experiments as well as the simulated effluent concentrations and fluxes from the vertical transport scenarios are available at a data repository (https:/doi.org/10.11583/DTU.11591106). This work was funded by the Ministry of Environment and Food of Denmark (CLAYFRAC project). The authors wish to thank the colleagues in the CLAYFRAC and PESTPORE projects for fruitful discussions. Constructive comments from three reviewers and from the Associate Editor helped improving the quality of the manuscript.

References

Albers, C. N., Ernstsen, V., & Johnsen, A. R. (2018). Soil Domain and Liquid Manure Affect Pesticide Sorption in Macroporous Clay Till. *Journal of Environment Quality*, *48*(1), 147. https://doi.org/10.2134/jeq2018.06.0222

Allaire, S. E., Gupta, S. C., Nieber, J., & Moncrief, J. F. (2002). Role of macropore continuity and tortuosity on solute transport in soils: 1. Effects of initial and boundary conditions. *Journal of Contaminant Hydrology*, *58*(3–4), 299–321. https://doi.org/10.1016/S0169-7722(02)00035-9

Batany, S., Peyneau, P. E., Lassabatère, L., Béchet, B., Faure, P., & Dangla, P. (2019). Interplay between molecular diffusion and advection during solute transport in macroporous media. *Vadose Zone Journal*, *18*(1). https://doi.org/10.2136/vzj2018.07.0140

Blessent, D., Jørgensen, P. R., & Therrien, R. (2014). Comparing Discrete Fracture and Continuum Models to Predict Contaminant Transport in Fractured Porous Media. *Groundwater*, *52*(1), 84–95. https://doi.org/10.1111/gwat.12032

Bradbury, K. R., Gotkowitz, M. B., Hart, D. J., Eaton, T. T., Cherry, J. A., Parker, B. L., & Borchardt, M. A. (2006). Contaminant Transport Through Aquitards: Technical Guidance for Aquitard Assessment, 1–143.

Broholm, M. M., Janniche, G. S., Mosthaf, K., Fjordbøge, A. S., Binning, P. J., Christensen, A. G., et al. (2016). Characterization of chlorinated solvent contamination in limestone using innovative FLUTe technologies in combination with other methods in a line of evidence approach. *Journal of Contaminant Hydrology*, *189*, 68–85. https://doi.org/10.1016/j.jconhyd.2016.03.007

Brusseau, M. L., Rao, P. S. C. C., Jessup, R. E., & Davidson, J. M. (1989). Flow Interruption: A Method for Investigating Sorption Nonequilibrium. *Journal of Contaminant Hydrology*, *4*(3), 223–240. https://doi.org/10.1016/0169-7722(89)90010-7

Carrera, J., Sánchez-Vila, X., Benet, I., Medina, A., Galarza, G., & Guimerà, J. (1998). On matrix diffusion: formulations, solution methods and qualitative effects. *Hydrogeology Journal*, *6*(1), 178–190. https://doi.org/10.1007/s100400050143

Chambon, J. C., Broholm, M. M., Binning, P. J., & Bjerg, P. L. (2010). Modeling multi-component transport and enhanced anaerobic dechlorination processes in a single fracture-clay matrix system. *Journal of Contaminant Hydrology*, *112*(1–4), 77–90. https://doi.org/10.1016/j.jconhyd.2009.10.008

Chapman, S. W., & Parker, B. L. (2005). Plume persistence due to aquitard back diffusion following dense nonaqueous phase liquid source removal or isolation. *Water Resources*

Research, *41*(12), 1–16. https://doi.org/10.1029/2005WR004224

Chapman, S. W., Cherry, J. A., & Parker, B. L. (2018). Multiple-scale hydraulic characterization of a surficial clayey aquitard overlying a regional aquifer in Louisiana. *Journal of Hydrology*, *558*, 546–563. https://doi.org/10.1016/j.jhydrol.2018.01.059

Cherry, J. A., Parker, B. L., Bradbury, K. R., Eaton, T. T., Gotkowitz, M. B., Hart, D. J., & Borchardt, M. A. (2006). *Contaminant transport through aquitards: A state-of-the-science review*. Denver.

Council of the European Union. (1998). Council Directive 98/83/EC of 3 November 1998 on the quality of water intended for human consumption. *Official Journal of the European Communities*, *L 330*, 32–54.

Cussler, E. L. (2009). *Diffusion: Mass transfer in fluid systems*. Cambridge: Cambridge University Press.

Fjordbøge, A. S., Janniche, G. S., Jørgensen, T. H., Grosen, B., Wealthall, G., Christensen, A. G., et al. (2017). Integrity of Clay Till Aquitards to DNAPL Migration: Assessment Using Current and Emerging Characterization Tools. *Groundwater Monitoring and Remediation*, (9999), 1–17. https://doi.org/10.1111/gwmr.12217

Flury, M., & Flühler, H. (1995). Tracer Characteristics of Brilliant Blue FCF. *Soil Science Society of America Journal*, *59*(1), 22. https://doi.org/10.2136/sssaj1995.03615995005900010003x

Fredericia, J. (1990). Saturated hydraulic conductivity of clayey tills and the roles of fractures. *Nordic Hydrology*, *21*, 119–132.

Grisak, G. E., & Pickens, J. F. (1980). Solute transport through fractured media - 1. The effect of matrix diffusion. *Water Resources Research*, *16*(4), 719–730.

Harrar, W. G., Murdoch, L. C., Nilsson, B., & Klint, K. E. S. (2007). Field characterization of vertical bromide transport in a fractured glacial till. *Hydrogeology Journal*, *15*(8), 1473–1488. https://doi.org/10.1007/s10040-007-0198-5

Harrison, B., Sudicky, E. A., & Cherry, J. A. (1992). Numerical analysis of solute migration through fractured clayey deposits into underlying aquifers. *Water Resources Research*, *28*(2), 515–526. https://doi.org/10.1029/91WR02559

Helmke, M. F., Simpkins, W. W., & Horton, R. (2005a). Ground water quality: Fracture-controlled nitrate and atrazine transport in four Iowa till units. *Journal of Environmental Quality*, *34*(1), 227–236. https://doi.org/10.2134/jeq2005.0227

Helmke, M. F., Simpkins, W. W., & Horton, R. (2005b). Simulating conservative tracers in fractured till under realistic timescales. *Ground Water*, *43*(6), 877–889. https://doi.org/10.1111/j.1745-6584.2005.00129.x

Høyer, A. S., Klint, K. E. S., Fiandaca, G., Maurya, P. K., Christiansen, A. V., Balbarini, N., et al. (2019). Development of a high-resolution 3D geological model for landfill leachate risk assessment. *Engineering Geology*, *249*(March 2018), 45–59. https://doi.org/10.1016/j.enggeo.2018.12.015

Jin, B., Rolle, M., Li, T., & Haderlein, S. B. (2014). Diffusive fractionation of BTEX and chlorinated ethenes in aqueous solution: Quantification of spatial isotope gradients. *Environmental Science and Technology*, *48*(11), 6141–6150. https://doi.org/10.1021/es4046956

Jørgensen, P. R., & Fredericia, J. (1992). Migration of nutrients, pesticides and heavy metals

in fractured clayey till. *Géotechnique*, *42*, 67–77.

Jørgensen, P. R., Broholm, K., Sonnenborg, T. O., & Arvin, E. (1998). DNAPL transport through marcroporous, clayey till columns. *Ground Water*, *36*, 651–660.

Jørgensen, P. R., McKay, L. D., & Spliid, N. H. (1998). Evaluation of chloride and pesticide transport in a fractured clayey till using large undisturbed columns and numerical modeling. *Water Resources Research*, *34*(4), 539–553.

Jørgensen, P. R., Hoffmann, M., Kistrup, J. P., Bryde, C., Bossi, R., & Villholth, K. G. (2002). Preferential flow and pesticide transport in a clay-rich till : Field, laboratory, and modeling analysis. *Water Resources Research*, *38*(11). https://doi.org/10.1029/2001WR000494

Jørgensen, P. R., McKay, L. D., & Kistrup, J. P. (2004). Aquifer vulnerability to pesticide migration through till aquitards. *Ground Water*, *42*(6), 841–855. https://doi.org/10.1111/j.1745-6584.2004.t01-3-.x

Jørgensen, P. R., Urup, J., Helstrup, T., Jensen, M. B., Eiland, F., & Vinther, F. P. (2004). Transport and reduction of nitrate in clayey till underneath forest and arable land. *Journal of Contaminant Hydrology*, *73*(1–4), 207–26. https://doi.org/10.1016/j.jconhyd.2004.01.005

Jørgensen, P. R., Spliid, N. H., Laier, T., & Outzen, S. (2016). Fate of Point-Source Pesticide Spill in Clayey Till after 15 Years. *Groundwater Monitoring and Remediation*, *36*(3), 33–42. https://doi.org/10.1111/gwmr.12153

Jørgensen, P. R., Mosthaf, K., & Rolle, M. (2019). A Large Undisturbed Column Method to Study Flow and Transport in Macropores and Fractured Media. *Groundwater*, *57*(6), 951–961. https://doi.org/10.1111/gwat.12885

Keller, C. K., Van Der Kamp, G., & Cherry, J. A. (1988). Hydrogeology of two Saskatchewan tills, I. Fractures, bulk permeability, and spatial variability of downward flow. *Journal of Hydrology*, *101*(1–4), 97–121. https://doi.org/10.1016/0022-1694(88)90030-3

Kessler, T. C., Klint, K. E. S., Nilsson, B., & Bjerg, P. L. (2012). Characterization of sand lenses embedded in tills. *Quaternary Science Reviews*, *53*(C), 55–71. https://doi.org/10.1016/j.quascirev.2012.08.011

Kim, E. K., Kang, Y. W., Christy, A. D., & Weatherington-Rice, J. (2017). Predicting fractures in glacially related fine-grained materials and a synthetic soil of bentonite and sand using soil texture. *Engineering Geology*, *222*, 84–91. https://doi.org/10.1016/j.enggeo.2017.03.007

Koestel, J., & Larsbo, M. (2014). Imaging and quantification of preferential solute transport in soil macropores. *Water Resources Research*, *50*, 4357–4378. https://doi.org/10.1002/2014WR015351

Lipson, D. S., Kueper, B. H., & Gefell, M. J. (2005). Matrix diffusion-derived plume attenuation in fractured bedrock. *Ground Water*, *43*(1), 30–39. https://doi.org/10.1111/j.1745-6584.2005.tb02283.x

Looms, M. C., Klotzsche, A., van der Kruk, J., Larsen, T. H., Edsen, A., Tuxen, N., et al. (2018). Mapping sand layers in clayey till using crosshole ground-penetrating radar. *Geophysics*, *83*(1), A21–A26. https://doi.org/10.1190/GEO2017-0297.1

Malaguerra, F., Albrechtsen, H. J., Thorling, L., & Binning, P. J. (2012). Pesticides in water

supply wells in Zealand, Denmark: A statistical analysis. *Science of the Total Environment*, *414*, 433–444. https://doi.org/10.1016/j.scitotenv.2011.09.071

Mckay, L. D., & Fredericia, J. (1995). Distribution, origin, and hydraulic influence of fractures in glacial deposit. *Canadian Geotechnical Journal*, *32*, 957–975.

McKay, L. D., Cherry, J. A., & Gillham, R. W. (1993). Field experiments in a fractured clay till, 1. Hydraulic conductivity and fracture aperture. *Water Resources Research*, *29*(12), 3879-389–0. Retrieved from http://onlinelibrary.wiley.com/doi/10.1029/92WR02592/full

McKay, L. D., Gillham, R. W., & Cherry, J. A. (1993). Field experiments in a fractured clay till: 2. Solute and colloid transport. *Water Resources Research*, *29*(12), 3879–3890. https://doi.org/10.1029/93WR02069

Mosthaf, K., Brauns, B., Fjordbøge, A. S., Rohde, M. M., Kerrn-Jespersen, H., Bjerg, P. L., et al. (2018). Conceptualization of flow and transport in a limestone aquifer by multiple dedicated hydraulic and tracer tests. *Journal of Hydrology*, *561*, 532–546. https://doi.org/10.1016/j.jhydrol.2018.04.011

Muniruzzaman, M., & Rolle, M. (2019). Multicomponent Ionic Transport Modeling in Physically and Electrostatically Heterogeneous Porous Media With PhreeqcRM Coupling for Geochemical Reactions. *Water Resources Research*, (Il). https://doi.org/10.1029/2019WR026373

Muniruzzaman, M., Haberer, C. M., Grathwohl, P., & Rolle, M. (2014). Multicomponent ionic dispersion during transport of electrolytes in heterogeneous porous media: Experiments and model-based interpretation. *Geochimica et Cosmochimica Acta*, *141*, 656–669. https://doi.org/10.1016/j.gca.2014.06.020

Nilsson, B., Sidle, R. C., Klint, K. E., Bøggild, C. E., & Broholm, K. (2001). Mass transport and scale-dependent hydraulic tests in a heterogeneous glacial till-sandy aquifer system. *Journal of Hydrology*, *243*(3–4), 162–179. https://doi.org/10.1016/S0022-1694(00)00416-9

O'Hara, S. K., Parker, B. L., Jørgensen, P. R., & Cherry, J. A. (2000). Trichloroethene DNAPL flow and mass distribution in naturally fractured clay: Evidence of aperture variability. *Water Resources Research*, *36*(1), 135–147. https://doi.org/10.1029/1999WR900212

Parker, B. L., Gillham, R. W., & Cherry, J. A. (1994). Diffusive disappearnacne of immiscible-phase organic liquids in fractured geologic media. *Ground Water*, *32*(5), 805–820.

Parker, B. L., Chapman, S. W., & Guilbeault, M. A. (2008). Plume persistence caused by back diffusion from thin clay layers in a sand aquifer following TCE source-zone hydraulic isolation. *Journal of Contaminant Hydrology*, *102*(1–2), 86–104. https://doi.org/10.1016/j.jconhyd.2008.07.003

Parker, B. L., Chapman, S. W., Goldstein, K. J., & Cherry, J. A. (2019). Multiple lines of field evidence to inform fracture network connectivity at a shale site contaminated with dense non-aqueous phase liquids. *Geological Society Special Publication*, *479*(1), 101–127. https://doi.org/10.1144/SP479.8

Rolle, M., & Kitanidis, P. K. (2014). Effects of compound-specific dilution on transient transport and solute breakthrough: A pore-scale analysis. *Advances in Water Resources*, *71*, 186–199. https://doi.org/10.1016/j.advwatres.2014.06.012

Rolle, M., Eberhardt, C., Chiogna, G., Cirpka, O. A., & Grathwohl, P. (2009). Enhancement of dilution and transverse reactive mixing in porous media: Experiments and model-based interpretation. *Journal of Contaminant Hydrology*, *110*(3–4), 130–142. https://doi.org/10.1016/j.jconhyd.2009.10.003

Rolle, M., Chiogna, G., Hochstetler, D. L., & Kitanidis, P. K. (2013). On the importance of diffusion and compound-specific mixing for groundwater transport: An investigation from pore to field scale. *Journal of Contaminant Hydrology*, *153*, 51–68. https://doi.org/10.1016/j.jconhyd.2013.07.006

Rolle, M., Sprocati, R., Masi, M., Jin, B., & Muniruzzaman, M. (2018). Nernst-Planck-based Description of Transport, Coulombic Interactions, and Geochemical Reactions in Porous Media: Modeling Approach and Benchmark Experiments. *Water Resources Research*, *54*(4), 3176–3195. https://doi.org/10.1002/2017WR022344

Rosenbom, A. E., Ernstsen, V., Flühler, H., Jensen, K. H., Refsgaard, J. C., & Wydler, H. (2008). Fluorescence imaging applied to tracer distributions in variably saturated fractured clayey till. *Journal of Environmental Quality*, *37*(2), 448–458. https://doi.org/Doi 10.2134/Jeq2007.0145

Sale, T., Parker, B. L., Newell, C. J., & Devlin, J. F. (2013). *Management of Contaminants Stored in Low Permeability Zones: A State-of-the-Science Review*.

Sidle, R. C., Nilsson, B., Hansen, M., & Fredericia, J. (1998). Spatially varying hydraulic and solute transport characteristics of a fractured till determined by field tracer tests, Funen, Denmark. *Water Resources Research*, *34*(10), 2515–2527. https://doi.org/10.1029/98WR01735

Snow, D. T. (1969). Anisotropic permeability of fractured media. *Water Resources Research*, *5*(6), 1273–1289.

Thorling, L., Ditlefsen, C., Ernstsen, V., Hansen, B., Johnsen, A. R., & Troldborg, L. (2019). *Grundvandsovervågning. Status og udvikling 1989-2018*. Retrieved from https://www.geus.dk/media/22917/grundvand1989-2018-rettet.pdf

Wang, L., Cardenas, M. B., Deng, W., & Bennett, P. C. (2012). Theory for dynamic longitudinal dispersion in fractures and rivers with Poiseuille flow. *Geophysical Research Letters*, *39*(5), 1–5. https://doi.org/10.1029/2011GL050831

Weatherill, D., Graf, T., Simmons, C. T., Cook, P. G., Therrien, R., & Reynolds, D. A. (2008). Discretizing the fracture-matrix interface to simulate solute transport. *Groundwater*, *46*(4), 606–615. https://doi.org/10.1111/j.1745-6584.2007.00430.x

Witherspoon, P. A., Wang, J. S. Y., Iwai, K., & Gale, J. E. (1980). Validity of cubic law for fluid flow in a deformable rock fracture. *Water Resources Research*, *16*(6), 1016–1024.

Worch, E. (1993). A new equation for the calculation of diffusion coefficients for dissolved substances. *Vom Wasser*, *81*, 289–297.

Ye, Y., Chiogna, G., Cirpka, O. A., Grathwohl, P., & Rolle, M. (2015a). Enhancement of plume dilution in two-dimensional and three-dimensional porous media by flow focusing in high-permeability inclusions. *Water Resources Research*, *51*, 5582–5602. https://doi.org/10.1002/2015WR016962

Ye, Y., Chiogna, G., Cirpka, O. A., Grathwohl, P., & Rolle, M. (2015b). Experimental Evidence of Helical Flow in Porous Media. *Physical Review Letters*, *115*(19), 1–5. https://doi.org/10.1103/PhysRevLett.115.194502

Young, N. L., Simpkins, W. W., Reber, J. E., & Helmke, M. F. (2019). Estimation of the representative elementary volume of a fractured till: a field and groundwater modeling approach. *Hydrogeology Journal*, *28*(2), 781–793. https://doi.org/10.1007/s10040-019-02076-y

Young, N. L., Simpkins, W. W., & Horton, R. (2021). Are Visible Fractures Accurate Predictors of Flow and Mass Transport in Fractured Till? *Groundwater*, *59*(1), 24–30. https://doi.org/10.1111/GWAT.13013

Yu, R., Andrachek, R. G., Lehmicke, L. G., Pierce, A. A., Parker, B. L., Cherry, J. A., & Freedman, D. L. (2018). Diffusion-Coupled Degradation of Chlorinated Ethenes in Sandstone: An Intact Core Microcosm Study. *Environmental Science & Technology*, acs.est.8b04144. https://doi.org/10.1021/acs.est.8b04144

Zheng, C., & Bennett, G. D. (2002). *Applied Contaminant Transport Modeling*. New York: John Wiley & Sons.